

Characterization of New Silicon Photomultipliers with Low Dark Noise at Low Temperature

K. Ozaki,^a S. Kazama,^{b,c} M. Yamashita,^a Y. Itow,^{a,b} S. Moriyama^{d,e}

^a*Institute for Space-Earth Environmental Research, Nagoya University, Nagoya, Aichi, 464-8601, Japan*

^b*Kobayashi-Maskawa Institute for the Origin of Particles and the Universe, Nagoya University, Nagoya, Aichi, 464-8601, Japan*

^c*Institute for Advanced Research, Nagoya University, Nagoya, Aichi 464-8601, Japan*

^d*Institute for Cosmic Ray Research, University of Tokyo, Kashiwa, Chiba 277-8582, Japan*

^e*Kavli Institute for the Physics and Mathematics of the Universe, Kashiwa, Chiba 277-8583, Japan*

E-mail: ozaki.kosuke@isee.nagoya-u.ac.jp, kazama@isee.nagoya-u.ac.jp

ABSTRACT: Silicon photomultipliers (SiPMs) have a low radioactivity, compact geometry, low operation voltage, and reasonable photo-detection efficiency for vacuum ultraviolet light (VUV). Therefore it has the potential to replace photomultiplier tubes (PMTs) for future dark matter experiments with liquid xenon (LXe). However, SiPMs have nearly two orders of magnitude higher dark count rate (DCR) compared to that of PMTs at the LXe temperature (~ 165 K). This type of high DCR mainly originates from the carriers that are generated by band-to-band tunneling effect. To suppress the tunneling effect, we have developed a new SiPM with lowered electric field strength in cooperation with Hamamatsu Photonics K. K. and characterized its performance in a temperature range of 153 K to 298 K. We demonstrated that the newly developed SiPMs had 6–54 times lower DCR at low temperatures compared to that of the conventional SiPMs.

KEYWORDS: Dark Matter detectors (WIMPs, axions, etc.); Photon detectors for UV, visible and IR photons (solid-state); Solid state detectors

Contents

1	Introduction	1
2	New SiPM with lowered electric field strength	2
3	Experimental setup	3
4	Measurements and Results	3
4.1	Gain vs voltages, breakdown voltage, and single photoelectron spectrum	3
4.2	Dark count rate and cross-talk probability	5
5	Conclusion and Outlook	7

1 Introduction

In the past three decades, numerous terrestrial experiments have been conducted to search for a faint interaction between weakly interacting massive particles (WIMPs) and ordinary matter. Among them, experiments using dual-phase (liquid/gas) xenon time projection chambers (TPCs) are leading the search for WIMPs with masses ranging from a few GeV/c^2 to a few TeV/c^2 [1–4]. For future experiments with larger detector mass such as DARWIN [5], it is important to further decrease the backgrounds for reaching the sensitivity limited by atmospheric and supernova relic neutrinos (neutrino floor) [6]. In the current experiments with liquid xenon (LXe), photomultiplier tubes (PMTs) were used to detect the prompt primary scintillation (S1) with a wavelength of ~ 175 nm [7] and secondary electro-luminescence of ionized electrons (S2), which are generated following an interaction between a WIMP and a xenon nucleus. However, PMTs have several important shortcomings, namely, their residual radioactivity levels [8, 9], bulkiness, and stability at cryogenic temperatures [10]. Therefore several alternative technologies are under consideration for future dark matter experiments with LXe. Recently, Silicon photomultipliers (SiPMs), sensitive to vacuum ultraviolet light (VUV), have been developed by Hamamatsu Photonics K. K. [11] and Fondazione Bruno Kessler [12]. It was reported that one of these SiPMs (Hamamatsu S13371 [13]) exhibited low intrinsic radioactivity [14]. Therefore SiPMs have the potential to replace PMTs for direct dark matter experiments. However, as listed in table 1, currently available SiPM has a high dark count rate (DCR) of $0.1\text{--}0.8$ Hz/mm^2 at the LXe temperature (~ 165 K) [15], which is $O(10\text{--}100)$ times higher than that for PMTs (Hamamatsu R11410) used in the current dark matter experiments with LXe [16]. Such a high DCR of SiPMs can generate numerous fake S1 signals due to accidental coincidences. In the XENON1T experiment, 3-fold coincidence with 100 ns time-window is required to create S1 signals [17]. Assuming the same requirement is applied for a future multi-ton LXe experiment with 1900 PMTs [5], this would result in an accidental coincidence rate of $O(1)$ Hz for PMTs, which is similar to the fake S1 rate observed in the XENON1T experiment [18].

Therefore it is necessary to reduce the DCR of SiPMs at least to the level achieved for PMTs ($\sim 0.01 \text{ Hz/mm}^2$) for low energy threshold and background level [19].

Table 1. Detector parameters for SiPMs and PMTs used in LXe experiments [13, 15, 16].

Photo-sensor	SiPM S13370	PMT R11410-21
Operation voltage	$\sim 50 \text{ V}$	$\sim 1500 \text{ V}$
Single photoelectron gain	$\sim 2 \times 10^6$	$\sim 5 \times 10^6$
Photo-detection efficiency at 175 nm	$\sim 24 \%$	$\sim 35 \%$
DCR at LXe temperature ($\sim 165 \text{ K}$)	$0.1\text{--}0.8 \text{ Hz/mm}^2$	$\sim 0.01 \text{ Hz/mm}^2$

2 New SiPM with lowered electric field strength

We developed a new SiPM (S12572-015C-SPL, which is hereafter referred as SPL) as a prototype sensor with a lower DCR in cooperation with Hamamatsu. This SiPM is similar to the commercially available SiPM (S12572-015C-STD, which is hereafter referred as STD [20]), but its internal electric field structure was modified to reduce the DCR as in [12]. Dark pulses of SiPMs mainly originate from the carriers generated thermally [21] and by the band-to-band tunneling effect [22]. The first component has a strong temperature dependence, while the second one has a weak dependence on temperature [23]. The high DCR of SiPM near the LXe temperature originates from the carriers due to the band-to-band tunneling, and the lowering of the internal electric field strength can suppress its effect, which enables to reduce the DCR [24]. Table 2 shows the comparison of detector parameters for SPL and STD. From the table we see that SPL and STD have the same properties of the active area, number of pixels, pixel pitches, and fill factor. Also, we can see from the table that operation voltage and single photoelectron (p.e.) gain are different because of the modified electric field structure. It is noted from table 2 that both the SiPMs are not sensitive to VUV light.

Table 2. Comparison of detector parameters between S12572-015C-SPL and S12572-015C-STD.

SiPM	S12572-015C-SPL	S12572-015C-STD
Operation voltage	$\sim 100 \text{ V}$	$\sim 65 \text{ V}$
Gain at over-voltage = 6 V	1.6×10^5	2.0×10^5
Active area	$3 \text{ mm} \times 3 \text{ mm}$	
Number of pixel	40000	
Pixel pitches	$15 \mu\text{m}$	
Fill factor	53 %	
Trench	No trench	
Spectral response range	$320 - 900 \text{ nm}$	

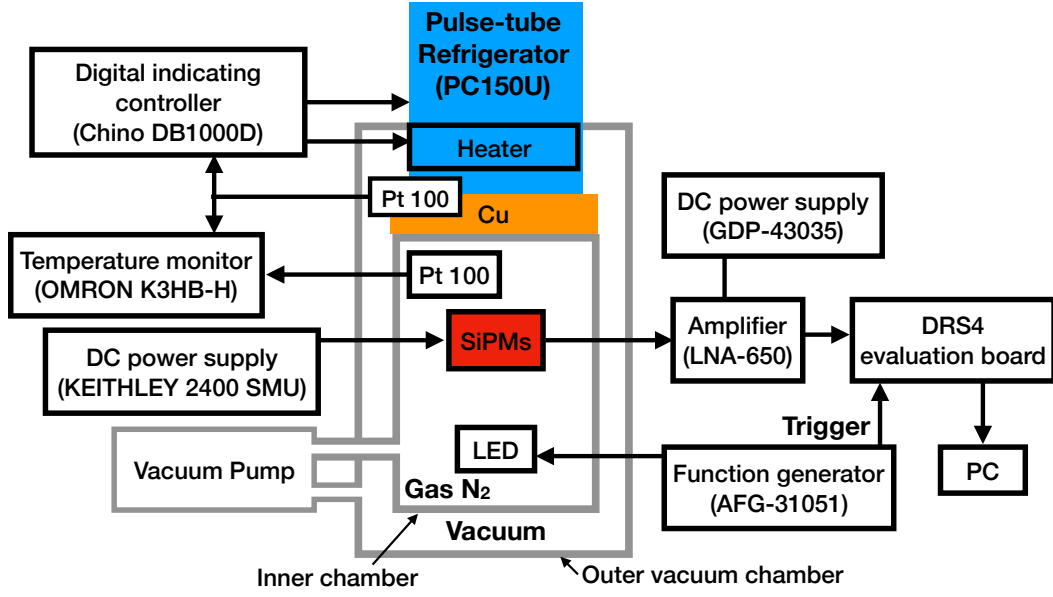


Figure 1. Block diagram of the setup of this experiment.

3 Experimental setup

The experiment was performed in the Kamioka underground laboratory at a depth of approximately 1,000 meters. Figure 1 shows a block diagram of the setup that was used for this experiment. This setup consisted of an inner chamber filled with gas nitrogen along with an outer vacuum chamber. SiPMs were installed in the inner chamber and on a readout board, and the readout schematic is shown in figure 2, left. Voltage (V_{bias}) from a source meter (KEITHLEY 2400 Source Meter) was applied to the SiPMs. Signals were amplified with a low noise amplifier (RF Bay LNA-650) and read out using a DRS4 evaluation board [25], which acquired data with a rate of 1 GS/s and a length of 1024 data points per time window. Square pulses from a function generator (Tektronix AFG-31051) were used to turn on an LED and trigger the data acquisition via the DRS4 board. We operated two SPLs labeled as SPL-1(-2) and two STDs labeled as STD-1(-2). Figure 2 (right), shows the typical waveforms of SPL-1 (STD-1) acquired with DRS4 at a temperature of 163 (164) K and bias voltages of 94.6 (60.0) V. Temperature was measured by two Pt-100 sensors and was controlled with a pulse-tube refrigerator (ULVAC CRYOGENICS PC150U) and a heater connected to a digital indicating controller (Chino DB1000D). We operated the setup at a temperature range of 153 K to 298 K, which was stable within ± 0.5 K during the measurements.

4 Measurements and Results

4.1 Gain vs voltages, breakdown voltage, and single photoelectron spectrum

To investigate the single p.e. gain, resolution, and breakdown voltage (V_{br}) properties of both SiPMs, we measured their responses to the blue light ($\lambda \sim 375$ nm) from an LED. The function

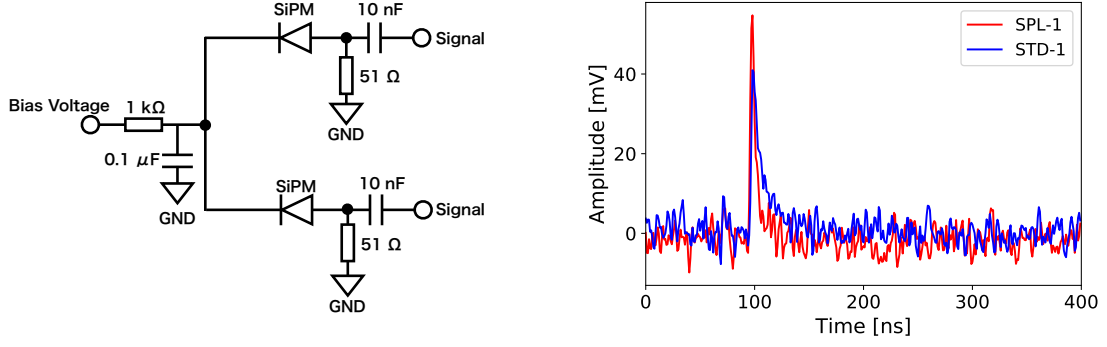


Figure 2. (Left): Readout schematic of SiPMs. It is possible to readout two SiPMs using a common bias voltage. (Right): Typical waveforms of single p.e. for SPL-1 (red) and STD-1 (blue) at a temperature of 163 K and 164 K, and a bias voltage of 94.6 V (SPL) and 60.0 V (STD), respectively.

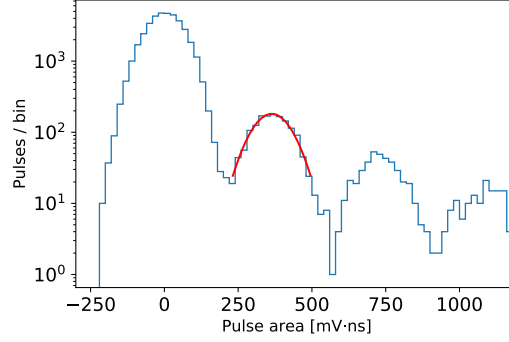


Figure 3. Pulse area spectrum of SPL-1 at a temperature of 163 K and a bias voltage of 94.6 V with a fitted Gaussian function (red line). The first and second peaks correspond to pedestal and single p.e., respectively.

generator inputs square pulses with a frequency of 460 Hz and a width of 30 ns to the LED. We obtained 40,000 triggered events for each temperature and bias voltage. Figure 3 shows a pulse area spectrum of SPL-1 at a temperature of 163 K and a bias voltage of 94.6 V.

At this temperature, single p.e. gains of SPL-1 and STD-1 at a bias voltage of 94.6 V (SPL) and 60.0 V (STD) are estimated to be 1.6×10^5 and 2.0×10^5 , respectively. The single p.e. resolutions ($\frac{\sigma_{1p.e.}}{\mu_{1p.e.}}$) of SPL-1 and STD-1 are measured to be 17.9 % and 18.8 %, respectively, where $\mu_{1p.e.}$ ($\sigma_{1p.e.}$) is mean (standard deviation) of the single p.e. pulse area obtained by fitting with Gaussian function as shown in figure 3. Figure 4 shows single p.e. gain of SPL-1 and STD-1 as a function of bias voltage. The single p.e. gain (G) can be expressed as

$$G = \frac{C_{\text{cell}}(V_{\text{bias}} - V_{\text{br}})}{q}, \quad (4.1)$$

where C_{cell} is a cell capacitance and q is an electric charge. The slope of a linearly fitted function in figure 4 corresponds to C_{cell}/q . The cell capacitance of SPL-1 and STD-1 are estimated to be 4.3 fF at 163 K and 5.4 fF at 164 K, respectively. Breakdown voltage (V_{br}), where the gain collapses to zero, is shown in figure 5 as a function of temperature. We can see from the figure 5

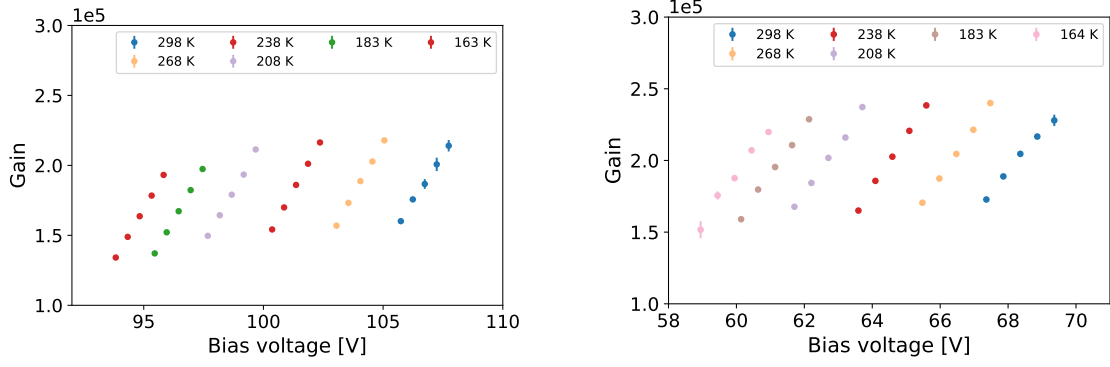


Figure 4. Single p.e. gain of SPL-1 (left) and STD-1 (right) as a function of bias voltage for temperatures ranging from 153 K to 298 K.

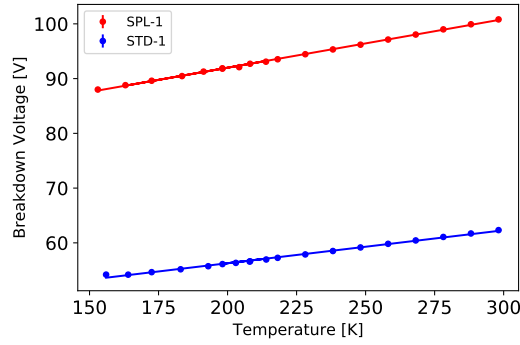


Figure 5. Breakdown voltage of SPL-1 and STD-1 as a function of temperature.

that V_{br} of SPL-1 and STD-1 decrease with a slope of 88.3 mV/K and 61.2 mV/K, respectively. Also, approximately at the LXe temperature, V_{br} of SPL-1 and STD-1 is estimated to be 88.8 V and 54.2 V, respectively. As discussed in section 2, V_{br} of SPL is higher than that of STD. For all the characteristics described above, no significant sample dependence is observed.

4.2 Dark count rate and cross-talk probability

DCR is defined as the number of pulses per second whose height is larger than 0.5 p.e. In this study, it was normalized by the active area and the fill factor for each SiPMs. At a temperature between 198 K and 298 K, we acquired data with random trigger because of high values of DCR. Below 198 K, data were obtained with self-trigger with a threshold of 25 mV. Figure 6 (left) shows a pulse height distribution of SPL-1 at 163 K and an over-voltage of 6.0 V, where over-voltage is defined as $V_{bias} - V_{br}$. The peak around 60 mV corresponds to the mean of the single p.e. pulse height. A red dashed line in figure 6 shows the self-trigger threshold of 25 mV. The remaining noise contribution is discarded by requiring that pulse area is larger than $\mu_{1p.e.} - 3\sigma_{1p.e.}$. For the data acquired with self-trigger, deadtime of the DRS4 evaluation board (~ 3 ms) is taken into account when calculating the DCR. Figure 6 (right) shows DCRs for SPL and STD that are expressed as a function of over-voltage at temperature of 298 K, 163 K(SPL), and 164 K(STD). DCR, as a function of temperature is also shown in figure 7 at over-voltages of 5.0 V and 7.0 V, respectively. As

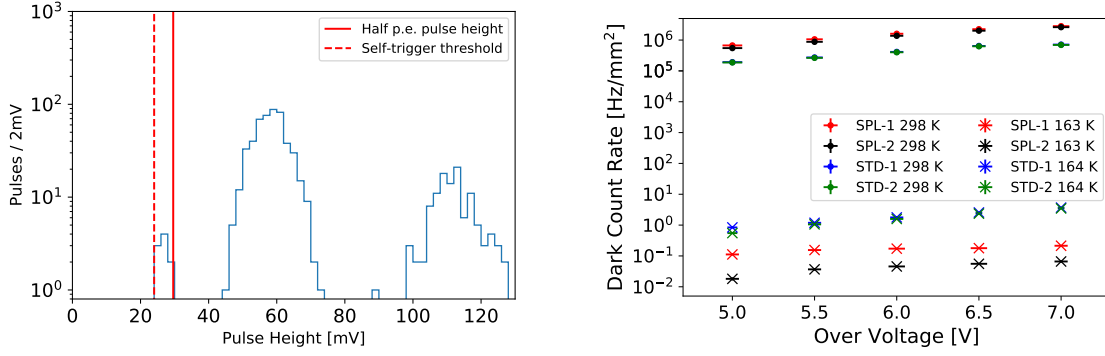


Figure 6. (Left): Pulse height distribution of SPL-1 acquired with self-trigger at a temperature of 163 K and an over-voltage of 6.0 V. Red dashed and solid lines show a self-trigger threshold of 25 mV and a half p.e. pulse height, respectively; (Right): Dark count rate of SPL and STD as a function of over-voltage at 298 K, 163 K (SPL), and 164 K (STD).

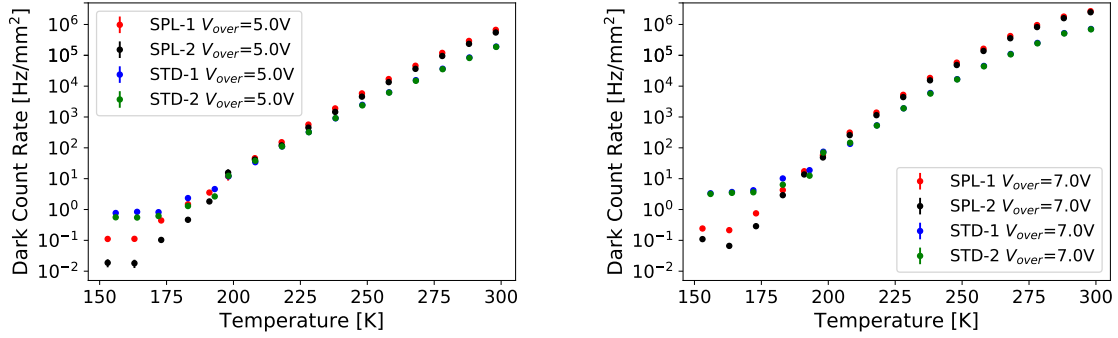


Figure 7. Dark count rate of SPL and STD as a function of temperature at over-voltages of 5 V (left) and 7 V (right).

discussed in section 2, between 200 K and 300 K, the contribution from thermally generated carriers is dominant; therefore, the DCR shows rapid decrease with temperature. However, at temperatures below 200 K, the contribution from carriers originating from the band-to-band tunneling effect is dominant; therefore, the DCR has less temperature dependence. The DCR for SPL-1(-2) at approximately 165 K is measured to be 0.11–0.24 (0.018–0.071) Hz/mm² depending on over-voltage, less by a factor of 6–54 compared with that of STD, indicating that the changing inner field structure reduced the DCR.

Cross-talk probability (CTP) is calculated as $\frac{N_{1.5}}{N_{0.5}}$, where $N_{1.5}$ and $N_{0.5}$ are the number of pulses per second whose pulse heights are larger than 1.5 p.e. and 0.5 p.e., respectively [26]. Cross-talk occurs when multiplied electrons in a cell enter and fire a neighboring cell. Figure 8 shows the CTPs for SPL and STD at different temperatures as a function of over-voltage. It can be seen from the figure 8 that CTP increases with over-voltage for both SiPMs but has a low temperature dependence. At approximately the LXe temperature and an over-voltage of 6.0 V, the CTPs of SPL-1 and STD-1 are estimated to be 33.4 % and 31.5 %, respectively. No significant sample differences in the CTP are observed.

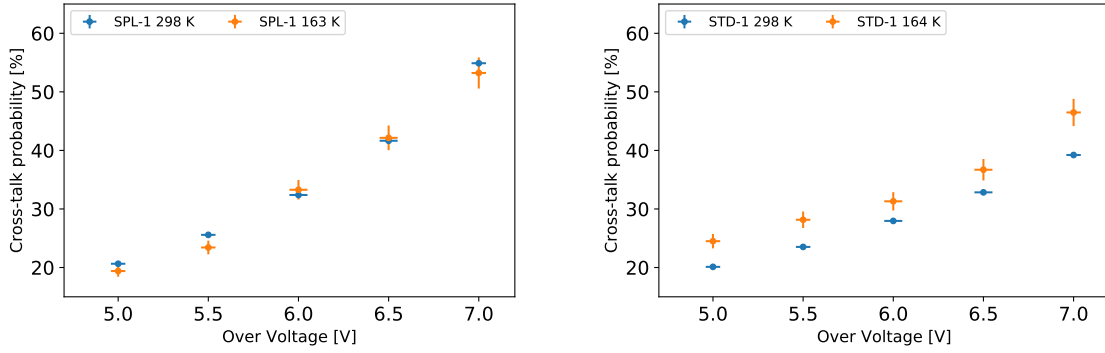


Figure 8. Cross-talk probability of SPL-1 (left) and STD-1 (right) as a function of over-voltage.

5 Conclusion and Outlook

SiPM is a good candidate for photo-detectors in future dark matter experiments with LXe because of its low radioactivity. However, it has a high DCR, and it is necessary to reduce it at least to the same level as it is for the PMTs (~ 0.01 Hz/mm²) used in LXe experiments [16]. With the help of Hamamatsu, we developed a dedicated SiPM (SPL) with lowered electric field for suppressing the band-to-band tunneling effect and operated it in a temperature range of 153–298 K. As a result, by modifying the inner electric field structure, the DCR at the LXe temperature could be reduced by a factor of 6–54 compared to that of STD that depended on over-voltage. Currently, both SPL and STD are not sensitive to the LXe scintillation light, but we are developing a dedicated SiPM sensitive to VUV light with the help of Hamamatsu. The DCR of S13370, a commercially available SiPM for VUV light detection, was measured to be 0.1–0.8 Hz/mm² at the LXe temperature depending on over-voltage [15]. With the same technology developed in this work, it might be possible that the DCR of S13370 can be reduced to the same extent, enabling SiPMs to be used in future dark matter experiments using LXe.

Acknowledgments

We thank Hamamatsu Photonics K. K. for this fruitful collaboration and the production of the SiPMs used in this study. We gratefully acknowledge the cooperation of Kamioka Mining and Smelting Company. This work was supported by DAIKO FOUNDATION, the Japanese Ministry of Education, Culture, Sports, Science and Technology, Grant-in-Aid for Scientific Research, JSPS KAKENHI Grant Number 19H05805 and 20H01931, and the joint research program of the Institute for Cosmic Ray Research (ICRR), the University of Tokyo.

References

- [1] E. Aprile et al. (XENON Collaboration), *Dark Matter Search Results from a One Ton-Year Exposure of XENON1T*, *Phys. Rev. Lett.* **121** 111302 (2018).
- [2] X. Cui et al. (PandaX-II Collaboration), *Dark Matter Results from 54-Ton-Day Exposure of PandaX-II Experiment*, *Phys. Rev. Lett.* **119** 181302 (2017).

- [3] D.S. Akerib et al. (LUX Collaboration), *Results from a Search for Dark Matter in the Complete LUX Exposure*, *Phys. Rev. Lett.* **118** 021303 (2017).
- [4] K. Abe et al. (XMASS Collaboration), *A direct dark matter search in XMASS-I*, *Physics Letters B* **789** (2019) 45–53.
- [5] J. Aalbers et al. (DARWIN Collaboration), *DARWIN: towards the ultimate dark matter detector*, *JCAP11* (2016) 017.
- [6] Ciaran A. J. O’Hare, *Dark matter astrophysical uncertainties and the neutrino floor*, *Phys. Rev. D* **94** 063527 (2016).
- [7] K. Fujii et al., *High-accuracy measurement of the emission spectrum of liquid xenon in the vacuum ultraviolet region*, *Nuclear Instruments and Methods in Physics Research A* **795** (2015) 293–297.
- [8] E. Aprile et al. (XENON Collaboration), *Lowering the radioactivity of the photomultiplier tubes for the XENONIT dark matter experiment*, *Eur. Phys. J. C* **75** 546 (2015).
- [9] K. Abe et al. (XMASS Collaboration), *Development of low radioactivity photomultiplier tubes for the XMASS-I detector*, *Nuclear Instruments and Methods in Physics Research Section A*, **922** (2019) 171–176.
- [10] E. Aprile et al. (XENON Collaboration), *The XENONIT Dark Matter Experiments*, *Eur. Phys. J. C* **77** 881 (2017).
- [11] S. Ogawa et al. (MEG II Collaboration), *Liquid xenon calorimeter for MEG II experiment with VUV-sensitive MPPCs*, *Nuclear Inst. and Methods in Physics Research, A* **845** (2017) 528–532.
- [12] F. Acerbi et al., *Silicon photomultipliers: technology optimizations for ultraviolet, visible and near-infrared range*, *Instruments*, 3(1), 15 (2019).
- [13] Hamamatsu Photonics,
https://www.hamamatsu.com/jp/ja/product/optical-sensors/mppc/mppc_mppc-array/index.html
- [14] L. Baudis et al., *Characterisation of Silicon Photomultipliers for Liquid Xenon Detectors*, 2018 *JINST* **13** P10022.
- [15] G. Gallina et al., *Characterization of the Hamamatsu VUV4 MPPCs for nEXO*, *Nuclear Inst. and Methods in Physics Research, A*, **940** (2019) 371–379.
- [16] P. Barrow et al., *Qualification tests of the R11410-21 photomultiplier tubes for the XENONIT detector*, 2017 *JINST* **12** P01024.
- [17] E. Aprile et al. (XENON Collaboration), *The XENONIT data acquisition system*, 2019 *JINST* **14** P07016.
- [18] E. Aprile et al. (XENON Collaboration), *XENONIT dark matter data analysis: Signal and background models and statistical inference*, *Phys. Rev. D* **99** 112009.
- [19] J. Wulf, *Direct Dark Matter Search with XENONIT and Developments for Multi-Ton Liquid Xenon Detectors*, Ph.D thesis, Universität Zürich (2018).
- [20] Hamamatsu Photonics,
https://www.hamamatsu.com/resources/pdf/ssd/s12572-010_etc_kapd1045j.pdf
- [21] G.A.M. Hurkx et al., *A New Analytical Diode Model Including Tunneling and Avalanche Breakdown*, *IEEE Trans. Electron Devices* **39** (1992) 2090–2098.
- [22] R.H. Haitz, *Mechanisms Contributing to the Noise Pulse Rate of Avalanche Diodes*, *J. Appl. Phys.* **36** (1965) 3123.

- [23] G. Collazuol et al., *Studies of silicon photomultipliers at cryogenic temperatures*, *Nuclear Inst. and Methods in Physics Research, A* **628** (2011) 389–392.
- [24] M. Ghioni et al., *Large-area low-jitter silicon single photon avalanche diodes*, *Quantum Sensing and Nanophotonic Devices V* **6900** (2008) 267–279.
- [25] PSI, DRS4 Evaluation Board, <https://www.psi.ch/en/drs/evaluation-board>
- [26] Hamamatsu Photonics, *Opto-semiconductor Handbook*,
https://www.hamamatsu.com/resources/pdf/ssd/e03_handbook_si_apd_mppc.pdf